analytical chemistry

Article

Cite This: Anal. Chem. 2018, 90, 2741−2748

pubs.acs.org/ac

NIR Phosphorescent Intramolecularly Bridged Benzoporphyrins and Their Application in Oxygen-Compensated Glucose Optode

Peter W. Zach,[†] Oliver T. Hofmann,[‡] Ingo Klimant,[†] and Sergey M. Borisov*[,†]

[†]Institute of Analytical Chemistry and Food Chemistry, Graz University of Technology, Stremayrgasse 9, 8010, Graz, Austria

[‡]Institute of Solid State Physics, Graz University of Technology, Petersgasse 16, 8010, Graz, Austria

Supporting Information

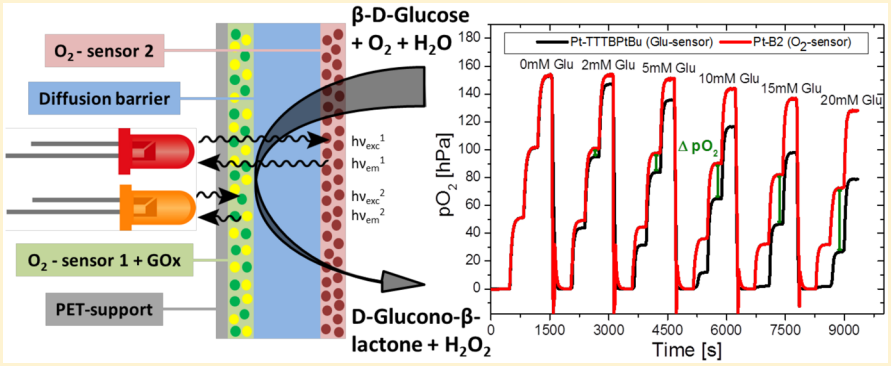

ABSTRACT: A glucose optode measuring the internal oxygen gradient is presented. The multilayer biosensor is composed of (i) analyte-impermeable transparent support, (ii) first oxygen-sensing layer combined with an enzymatic layer, (iii) diffusion barrier, and (iv) second oxygen-sensing layer. To make this design suitable for measurement in subcutaneous tissue, a pair of NIR phosphorescent indicators with very different spectral properties is chosen. Combination of a conventional Pt(II) tetrabenzoporphyrin dye (absorption and emission maxima at 617 and 772 nm, respectively) used in the first layer and a new intramolecularly bridged Pt(II) complex (absorption and emission maxima at 673 and 872 nm, respectively) in the second layer enables efficient separation of both emission signals. This specially designed dye class is accessible via Scholl-reaction from tetraphenyltetrabenzoporphyrin complexes. For the first time, the new optode allows simultaneous glucose and oxygen measurement in a single spot and therefore accurate compensation of oxygen heterogeneities resulting from fluctuations in the tissue. The presented material covers the dynamic ranges from 0 to 150 hPa O_2 and from 0 to 360 mg/dL (20 mM) glucose (at 37 °C).

Quantification of glucose is undoubtedly one of the most important analytical tasks today. Glucose is an important analyte in biotechnology, biology, and food industry, but sensing glucose in blood is definitely of highest interest.[1] Already in 2014, 8.5% of adults aged 18 years and older (422 million people) suffered from diabetes mellitus.[2] This chronic disease (inherited or acquired) is characterized by deficiency of the insulin production by the pancreas, or by the inefficiency of use of the produced insulin, resulting in a very high concentration of glucose in blood damaging especially the nerves and blood vessels.[2] Therefore, research on glucose measurement in blood in general and particularly on continuous glucose monitoring techniques (which in combination with an insulin pump makes artificial pancreas possible) has been a topic of great importance. Although electrochemical methods of glucose quantification are the most established ones,[3] optical sensing technology can provide an interesting alternative.[1] Optical sensors are cost-effective, enable simple design and handling, are easy to miniaturize and are free of electromagnetic interferences.[1] Several concepts of optical glucose monitoring make use of different types of recognition and utilize either natural receptors such as apoenzymes and lectins (concanavalin A)[4,5] or synthetic ones like boronic acids.[6] Another large group of sensors is based on monitoring of the formation or consumption of metabolites during enzymatic oxidation of glucose catalyzed by glucose oxidase (GOx).[7−9] These sensors benefit from very high selectivity for glucose over other saccharides.[7] Enzymatic glucose sensors based on oxygen optodes remain the most promising ones due high versatility and robustness of these transducers.[10] However, the signal of these sensors is affected by oxygen fluctuations in the sample, resulting in necessity of an additional detection of the oxygen partial pressure.[11] This, for instance, can be realized with help of an array of fiber-optic oxygen and glucose sensors.[11−13] Such solution, however, neither enables subcutaneous glucose

Received: November 17, 2017
Accepted: January 28, 2018
Published: January 29, 2018

DOI: 10.1021/acs.analchem.7b04760
Anal. Chem. 2018, 90, 2741−2748

monitoring through skin nor compensates for microheterogeneities in oxygen distribution in tissues.[14,15]

Evidently, conventional UV−vis indicators are not suitable for subcutaneous measurement due to strong light scattering by the tissue, efficient light absorption by skin pigments and hemoglobin as well as strong autofluorescence. Oxygen indicators operating in the so-called NIR optical window[16] overcome the above limitations.[17−19] Nacht et al.[20] reported a catheter-based array for continuous measurement of glucose and oxygen in subcutaneous tissue. Unfortunately, the overlapping absorption of the chosen indicator dyes (Pt(II) tetraphenylterabenzoporphyrin and aza-triphenyl-tetrabenzoporphyrin complexes) did not enable complete separation of the luminescence signals from the indicators. Additionally to the optical cross-talk, the glucose and the reference oxygen sensors were located at different parts of the infusion catheter, so that accurate compensation of the glucose measurement for oxygen variations was not possible. Furthermore, such configuration results in much lower signal for the sensor positioned closer to the end of the catheter due to its deeper position in the tissue.

In respect to minimization of the optical cross-talk, potential improvements are limited by availability of NIR oxygen indicators with acceptable photophysical properties. Particularly, despite large Stokes shift exceeding 200 nm, Pt(II) and Pd(II) aza-triphenyltetrabenzoporphyrins show only minor bathochromic shift of absorption compared to the parent tetraphenyltetrabenzoporphyrins.[21] On the other hand, the absorption maxima of the complexes of naphthoporphyrins[22] and their molecular hybrids with benzoporphyrins[23] can be extended up to 689 nm (Pt(II) tetraphenyltetranaphthoporphyrin),[24,25] but these dyes suffer from poor solubility and photostability[23] and synthetic routes to analogues with improved properties are challenging.[26]

In this contribution we report a new class of NIR phosphorescent emitters which are accessible via one-step modification of Pt(II) tetraphenyltetrabenzoporphyrin (TPTBP) in an intramolecular rigidization via Scholl reaction. Remarkable photophysical properties of the new dyes enable subcutaneous sensing of glucose and oxygen in combination with Pt(II) tetraphenyltetrabenzoporphyrin derivatives. Moreover, in order to ensure an even more accurate compensation of the glucose sensors we realized a new sensing concept in which both oxygen indicators are located in different layers of a single material separated by the enzymatic layer and a diffusion barrier.

EXPERIMENTAL SECTION

Materials and Methods. 1,2-Dichlorobenzene, poly(styrene-*co*-divinylbenzene)-microspheres (PS-DVB, 8 μm particle size), 1,4-diazabicyclo[2.2.2octane] (DABCO), 1,4-butandiol, poly(tetrahydrofuran) (poly(THF), average M_n ∼ 1000 g mol^{-1}), and glucose oxidase (EC 1.1.3.2 from *Aspergillus niger*, 200 U/mg) were ordered from Sigma-Aldrich and aluminum trichloride from Fluka. Molybdenum pentachloride, and di-*n*-butyldilauryltin were purchased from ABCR and silica-gel 60 from Merck. Polystyrene (PS; M_w = 260000 g mol^{-1}) was obtained from Acros Organics. Hydrogels Hydromed D4 and D7 were obtained from AdvanSource (www.advbiomaterials.com). Sodium sulfate, sodium dihydrogen phosphate, and sodium chloride were from VWR. Dicyclohexylmethane-4,4′-diisocyanate was purchased from TCI. All the solvents and triethylamine (TEA) were from Roth; anhydrous ethanol was from Fisher Scientific. Nitrogen (99.999% purity) was purchased from Air Liquide and oxygen (99.999% purity) from Linde Gas GmbH. Poly(ethyleneterephthalate) (PET) support Melinex 505 was purchased from Pütz (Taunusstein, Germany). Pt(II) tetraphenyltetrabenzoporphyrin (Pt-TPTBP) and Pt(II) tetratolyl-tetra-(*t*-butyl)tetrabenzo-porphyrin (Pt-TTTBPtBu) were synthesized analogously to the literature procedure,[27] with details provided in the Supporting Information.

Synthesis. *Synthesis of Pt-B1.* Pt-TPTBP (48.00 mg, 47.6 μmol, 1.00 equiv) was dissolved in 12 mL of 1,2-dichlorobenzene in a closed 25 mL round-bottom flask. Then aluminum trichloride (825.4 mg, 6.190 mmol, 130 equiv) was added and the solution was ultrasonicated for 10 min, resulting in a color change from dark-green to a brownish-red. The reaction mixture was quickly heated to 155 °C in an oil bath accompanied by bubbling of oxygen through the solution. The reaction progress was monitored via absorption spectra; the samples (10 μL) were neutralized with 30 μL of TEA and diluted with dichloromethane (DCM). After completion, the reaction mixture was allowed to cool to room temperature under continuous O_2-bubbling through the solution. The reaction mixture was neutralized with a DCM/TEA solution (40:1 v/v) and the obtained precipitate was removed via centrifugation. The solution was shaken with H_2O (3 × 100 mL) to remove the excess of TEA and dried over Na_2SO_4. The solvent was removed under reduced pressure. The product was purified via column chromatography (silica-gel) and subsequently washed with cyclohexane (3 × 15 mL), yielding a green solid. Yield: 4.3 mg, 9%. UV−vis absorption spectra: $\lambda_{max}/\varepsilon$ (nm/M^{-1} cm^{-1}) in toluene: 440/40.000; 455/45.000; 483/100.000; 606/7.000; 622/10.000; 641/20.000; 676/56.000. MALDI: m/z [M$^+$] $C_{60}H_{28}N_4Pt$: Calcd, 999.1967; found, 999.1927.

Synthesis of Pt-B2. Synthesis and purification of Pt-B2 was performed analogously to modification of Pt-TPTBP (1), but Pt-TTTBPtBu (48.00 mg, 35.5 μmol, 1.00 equiv) was used instead. A total of 48 mL of 1,2-dichlorobenzene and 614.8 mg (4.6 mmol, 130 equiv) of aluminum trichloride were used. Yield: Pt-B2 4.0 mg, 11%. Pt-B3 and Pt-B4 were isolated as byproducts with yields of 3.1 mg (8%) and 1.2 mg (3%), respectively (Supporting Information). UV−vis absorption spectra: $\lambda_{max}/\varepsilon$ (nm/M^{-1} cm^{-1}) in toluene: 443/42.000, 457/47.000, 485/110.000, 619/12.000, 640/23.000, 673/58.000.

Synthesis of Hydrophobic Polyurethane (PU-THF). Poly(THF) (1.00 g, 1.00 mmol, 1.00 equiv) and 1,4-butanediol (180 mg, 2.00 mmol, 2.00 equiv) were dissolved in 30 mL of dry THF in a Schlenk flask under argon atmosphere. The mixture was stirred for 10 min. Then dicyclohexylmethane-4,4′-diisocyanate (0.89 g, 3.4 mmol, 3.4 equiv), 1,4-diazabicyclo[2.2.2octane] (DABCO) (5 mg, 0.045 mmol), and di-*n*-butyldilauryltin (22 mg, 0.035 mmol) were added under argon atmosphere. The reaction mixture was heated to 60 °C and stirred for 16 h. After completion the reaction mixture was cooled down to room temperature and the polymer precipitated in 300 mL of a mixture of EtOH/H_2O (1:1 v/v), centrifuged, and then dried under vacuum oven at 75 °C for 24 h. Yield: 1.4 g. GPC analysis: M_n = 1.43 × 10^4 g mol^{-1}; M_w = 2.36 × 10^4 g mol^{-1}; M_w/M_n = 1.65; M_z = 3.38 × 10^4 g mol^{-1}, M_z/M_w = 1.43.

Immobilization of Pt-B2 and Pt-TTTBPtBu into PS-DVB Beads. A solution of 2 mg Pt-B2 in 1 mL of chloroform ($CHCl_3$) was slowly added to a 20% (w/v) dispersion of PS-

DOI: 10.1021/acs.analchem.7b04760
Anal. Chem. 2018, 90, 2741−2748

DVB microspheres in $CHCl_3$. The mixture was stirred for 10 min. Then, 3 mL of a mixture of ethanol (EtOH)/H_2O (1:1 v/v) were slowly added, followed by 10 min of stirring. The solvent was removed under reduced pressure, the residue redissolved in a mixture of EtOH/H_2O (4:1 v/v), then centrifuged twice, and dried in the vacuum oven at 75 °C for 24 h.

A solution of 5 mg Pt-TTTBPtBu in 1.5 mL of tetrahydrofuran (THF) was slowly added to a 20% (w/v) dispersion of PS-DVB beads in THF. The mixture was stirred for 10 min. Then 3 mL of H_2O were slowly added, followed by 10 min of stirring. The mixture was then poured into 40 mL H_2O, filtered, washed five times with a mixture of EtOH/H_2O (4:1 v/v), and dried in the vacuum oven at 75 °C for 24 h.

Preparation of the Oxygen Sensor. The sensor was prepared by knife-coating the "cocktail" containing 0.05 wt % Pt-B2 dye and 10 wt % of polystyrene in chloroform (HPLC-grade). After the coating, the sensor films were dried for 24 h at 60 °C to ensure complete removal of solvent.

Preparation of the Glucose Sensor. A total of 25 mg Pt-TTTBPtBu-PS-DVB microspheres and 50 mg D7 hydrogel were dispersed/dissolved in a mixture of 300 mg EtOH/H_2O (9:1 v/v) to obtain "cocktail 1". Meanwhile, 500 μL of EtOH was slowly added to the solution of 7.5 mg GOx in 150 μL of H_2O, which immediately turned cloudy. The GOx precipitate was centrifuged twice, dispersed in 100 μL of EtOH/H_2O (4:1 v/v) and mixed with the "cocktail 1" for 30 min. The mixture was knife coated on PET support (25 μm wet layer) that, prior to coating, was plasma-etched in an oxygen atmosphere using a Femto low-pressure plasma system form Diener electronic (Ebhausen, Germany). The solvents were allowed to evaporate at room temperature for 2 h. A total of 100 mg of PU-THF and 25 mg of D7 hydrogel were dissolved in 550 mg of EtOH/H_2O mixture (9:1 v/v) with the help of an ultrasonic finger (INULA; Vienna, Austria) using the following setting (duration overall: 3 min; amplitude: 15%; pulse on: 2 s; pulse off: 8 s), resulting in an opaque, colorless solution. This "cocktail" was then knife coated on the layer containing Pt-TTTBPtBu-PS-DVB and GOx (165 μm wet layer thickness). The foil was dried at RT for 3 h and a "cocktail" containing 10 mg of Pt-B2-PS-DVB microspheres, 15 mg of D7 hydrogel, and 85 mg EtOH/H_2O (9:1 v/v) was coated to produce the last layer. After evaporation of the solvents at RT, the foil was stored in the fridge at 5 °C in the darkness. The thickness of the knife-coated layers was determined using a Millimess 2000 Inductive Digital Comparator from Mahr (Göttingen, Germany).

Measurements. The absorption spectra were recorded on a CARY 50 UV−vis spectrophotometer from Varian. Luminescence spectra were recorded on a FluoroLog 3 spectrofluorometer from Horiba Scientific equipped with a NIR-sensitive R2658 photomultiplier from Hamamatsu. Determination of relative quantum yields was done according to Crosby and Demas using the solution of BF_2 chelate of [5-(4-buthoxyphenyl)-3-phenyl-1*H*-pyrrol-2-yl][5-(4-buthoxyphenyl)-3-phenylpyrrol-2-ylidene]amine in chloroform as a reference (Φ = 36%).[28] All dye solutions were deoxygenated in a screw-cap cuvette (Hellma; Müllheim, Germany) by bubbling argon through the solution for 10 min. Photophysical studies in solutions were performed for the dye concentrations between 2 and 4 × 10^{-6} mol·L^{-1}.

The phosphorescence decay times were acquired in frequency domain using a Firesting oxygen meter from PyroScience (Aachen, Germany) with a modulation frequency of 4 kHz. For characterization of the oxygen sensor, the composition of the gas was adjusted with a custom-build gas-mixing device based on mass-flow controllers from Voegtlin (Hamburg, Germany; www.red-y.com) by mixing compressed air, nitrogen, and oxygen. Temperatures were kept constant by a cryostat ThermoHaake DC50 (www.thermoscientific.de/home.html).

Characterization of the Glucose Sensor. All measurements were conducted in a climate cabinet (Memmert; Schwabach, Germany) at 37 °C. A round sensor spot with a diameter of 1 cm was punched out with a stamp (BGS technic; Wermelskirchen, Germany) and glued onto the inner wall of a 100 mL Schott bottle (2 cm above the bottle base) using vacuum fat. Optical read-out module BiLuMOS (described in detail by Nacht et al.[20] and modified here by replacing the 635 nm LED by a 670 nm LED) was positioned on the outer wall of the flask. The bottle was filled with 100 mL of a 150 mM NaCl solution, equipped with a magnetic stirring bar and sealed with a screw-cap containing a septum. A gas bubbler connected to a tube was positioned approximately 1 cm over the stirring bar, and an external thermometer (TFA Dostmann; Wertheim-Reicholzheim, Germany) and a cannula (for pressure compensation) were inserted through the septum. The solution was stirred at 500 rpm using a magnetic stirrer. The composition of the gas (0, 50, 100, and 150 hPa pO_2) was adjusted as described above for the oxygen sensor. The addition of the respective amount of glucose was done with a syringe and a cannula through the septum without opening the Schott bottle by using a glucose stock solution of 400 mg·mL^{-1}. Measurements were performed at 0, 2.4, 5.2, 10.5, 15, and 20 mM glucose.

RESULTS AND DISCUSSION

Synthesis of the New NIR Dyes. The precursors for the modification, Pt(II) complexes of tetraphenyltetrabenzoporphyrin (TPTBP) and its derivative bearing alkyl groups (Figure 1) are conveniently prepared in only three steps: formation of the Zn(II) complex in a modified template condensation,[27] demetalation in acidic media, and subsequent metalation of the

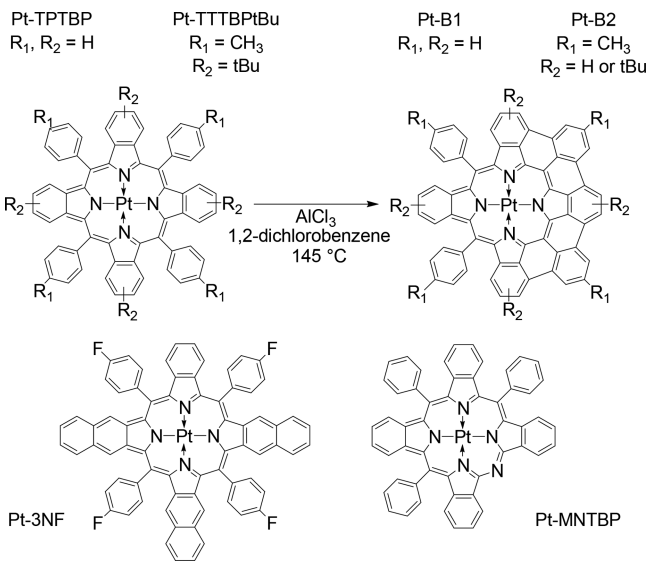

Figure 1. Chemical structures of precursors and bridged products Pt-B1 and Pt-B2 (according to DFT calculations), as well as reported Pt-3NF[23] and Pt-NTBP[21] NIR phosphorescent dyes.

DOI: 10.1021/acs.analchem.7b04760
Anal. Chem. 2018, 90, 2741−2748

metal-free porphyrin. Although the yields of Zn(II) porphyrins in template condensation are generally not high (5−10%), the method allows preparation of the dyes on multigram scale due to simplicity of the procedure and low cost of starting compounds. In TPTBPs, the *meso*-positioned aryl substituents are out of plane and therefore they only very minor affect the spectral properties of the dyes (bathochromic shift of the absorption of the Q-band by about 5 nm for each aryl substituent). We perceived that intramolecular bridging will prevent the rotation of these substituents and result in significant extension of the conjugation. Scholl reaction (oxidative coupling of aromatic moieties in the presence of Lewis acids such as $FeCl_3$, $AlCl_3$, $CuCl_2$)[29] was an evident choice to perform the intramolecular bridging of the benzoporphyrins. Although Scholl reaction is not common for fusion of different aromatic fragments in metal complexes, it is quite popular for modification of organic compounds.[30−32] Readily available Pt-TPTBP was chosen for the proof of concept experiments. The reaction was conducted in an oxidative atmosphere (bubbling O_2 through the solution) in 1,2-dichlorobenzene (bp 180.5 °C) in the presence of $AlCl_3$ as Lewis acid. The resulting bridged product was isolated with the help of column chromatography. Mass spectra (Figure S51, Supporting Information (SI)) revealed that the product Pt-B1 (Figure 1) was a mixture of 4-fold bridged compounds resulting from the loss of 8 protons, namely the expected reaction product (MW of PtTPTBP - 8) and side products, which showed the substitution with chlorine and/or chlorobenzene originating from the solvent. Unfortunately, chromatographic separation of these products was not successful. The attempts to use alternative Lewis acids ($MoCl_5$, $FeCl_3$) as well as solvents (chloroform, nitromethane, 1,2-dichloroethane, trimethylbenzene, diphenylsulfone) to avoid the undesired side reactions were not successful. In order to elucidate the bridging pattern of in the modified Pt-TPTBP compound, time-dependent density functional theory (TD-DFT) calculations were carried out for the precursor (Pt-TPTBP) and all the possible structures (Figure S16, SI). The calculations indicate (Figure S17, SI) that the structure presented in Figure 1 is the most likely from the 4-bridged species which can potentially form.

The bridged product Pt-B1 has significantly lower solubility than the precursor, because the increased planarity of the macrocycle favors aggregation via $\pi-\pi$-stacking. This is an evident disadvantage for practical applications; thus we tried to overcome this limitation by introducing alkyl groups in different positions of the benzoporphyrin macrocycle. Surprisingly, only traces of the bridged product were observed upon reaction of the Pt(II) complex bearing 8 methyl groups in β positions (Pt-TPTBPdM$_4$; Figure S3, SI) as indicated by the absorption spectra (Figure S20, SI). Low reactivity of the octamethyl complexes is likely to be due to sterical effects preventing formation of a stable intermediate with aluminum chloride. Another reason might be a good stabilization of the obtained cation by the two methyl-groups preventing the formation of the C−C bond. Scholl reaction of the Pt(II) *meso*-tetratolyltetrabenzoporphyrin complex bearing only four CH_3 groups in the β-positions (Figure S6, SI) indicated the formation of 4-fold bridged species, but no sufficient conversion could be achieved due rapid decomposition of the intermediates or the product (Figure S22, SI). The attempts to perform 4-fold bridging with the corresponding Zn(II) complex (Zn-TTTBPmM$_4$; Figure S7, SI) were not successful since only the monobridged complex was observed (Figures S21 and S48, SI). In contrast to Scholl reaction with the more stable Pt(II) complex, the Zn(II) complex is demetalated in the presence of $AlCl_3$ resulting in protonated metal-free porphyrin. Since the dication is less electron-rich compared to the metalated complex, the formation of further C−C bonds is prevented.

Finally, Scholl reaction with Pt(II) *meso*-tetra-tolyl-tetra-*tert*-butylbenzoporphyrin (Pt-TTTBPtBu) resulted in formation of the desired 4-bridged product (Pt-B2, Figure 1) along with two other differently bridged compounds (Pt-B3 and Pt-B4; (Figures S14, S53, and S54 and Table S1, SI), which were separated via column chromatography. The MS spectrum for bridged compound Pt-B2 (Figure S52, SI) indicates formation of 4-fold bridged species, accompanied by the loss of 1−4 tBu groups due to Friedel−Crafts dealkylation and addition of chlorine atoms. The methyl groups in the *meso*-position of the porphyrin macrocycle are retained, which positively affects the solubility of the resulting products making immobilization of the dye into polymers possible. Due to acceptable solubility, the new Pt-B2 dye was chosen for further application in oxygen and glucose sensors.

Photophysical Properties. Intramolecular bridging of benzoporphyrin derivatives via Scholl reaction leads to a remarkable bathochromic shift of the Soret band and the Q-band (Figure 2, Table 1). In fact, for Pt-B1 shifts of about 50 and 60 nm are observed for the Soret and the Q-band, respectively. Absorption and emission properties of the 4-fold

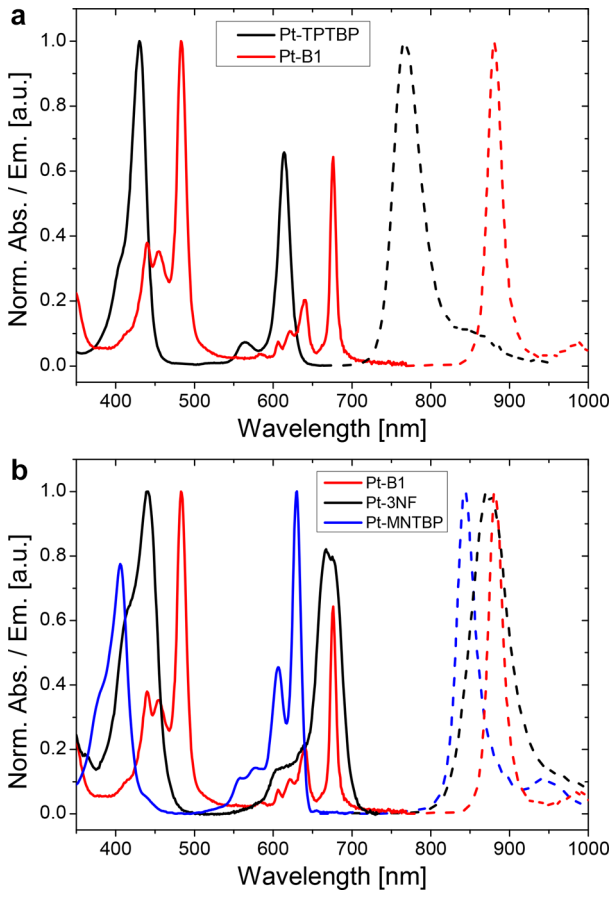

Figure 2. (a) Absorption (solid lines) and emission (dashed lines) spectra of Pt-TPTBP and bridged compound Pt-B1 in toluene. (b) Comparison of the spectral properties of Pt-B1 and reported NIR phosphorescent dyes with similar spectral properties.

DOI: 10.1021/acs.analchem.7b04760
Anal. Chem. 2018, 90, 2741−2748

Table 1. Photophysical Properties of Pt-B1 and the Reported NIR Metalloporphyrins in Anoxic Toluene

dye	abs_{max} λ [nm], ($\varepsilon \cdot 10^{-3}$ cm^{-1} M^{-1})	fwhm, Q-band [cm^{-1}][a]	Em λ_{max} [nm]	Stokes shift [cm^{-1}]	Φ [%]	τ [μs]
Pt-TPTBP	430 (205), 564 (16), 614 (136)	480	770	3300	20	47
Pt-B1	440 (40), 455 (45), 483 (100), 641 (20), 676 (56)	185	880	3430	7	39
Pt-3NF	441 (108), 618 (17.2), 635 (21.9), 667 (83.5), 678 (78.9)	775	870	3255	8	21
Pt-MNTBP	406 (106), 606 (61), 630 (137)	320	844	4025	9	40

[a]For the Q-band with the lowest energy.

bridged products obtained from Pt-TPTBP (Pt-B1) and Pt-TTTBPtBu (Pt-B2) as well as emission quantum yield Φ and lifetime τ (Tables 1 and S1 and Figure S14, SI) are virtually identical, indicating that peripheral substitution with the alkyl groups neither affects the bridging pattern nor the spectral properties. Interestingly, the Soret and the most intense Q-band for the 4-fold substituted products Pt-B1 and Pt-B2 (Figures 2 and S14, SI and Tables 1 and S1, SI) are much narrower than for the respective parent complexes (fwhm 185 and 480 cm^{-1} for Pt-B1 and Pt-TPTBP, respectively).

The bridged compounds are phosphorescent at room temperature (Figure 2, Table 1). Similarly to the absorption, the phosphorescence band is bathochromically shifted compared to the parent compound and is narrower. The S_1-T_1 energy gap is almost not affected by the bridging (ΔE = 3300 and 3430 cm^{-1} for Pt-TPTBP and Pt−B1, respectively). Lower energy of the triplet state is responsible for decrease of the phosphorescence quantum yields, which are nevertheless sufficiently high (Table 1). The phosphorescence decay times are only slightly smaller than for Pt-TPTBP.

Overall, the new dyes show rather similar photophysical properties to those of Pt(II) *meso*-tetraphenyltrinaphthoporphyrin Pt-3NF (Figure 1) in respect to position of the Q-band and the phosphorescence peak, and the emission quantum yields (Table 1). However, the absorption and emission bands of the new dyes are significantly narrower, which is favorable for efficient spectral separation in the multiparameter sensors. Both Pt-B1 and Pt-3NF show significantly longer absorption and emission maxima than the aza-triphenyltetrabenzoporphyrin Pt-MNTBP.

Photostability of the new dye class with that of the naphthoporphyrins was also compared. Since the Soret band of Pt-3NF showed poor compatibility with the emission of the high power blue LED array, the analogous Pd(II) complex was used (λ_{max} = 456 nm). As can be observed (Figure 3), the photostability of these two classes of oxygen indicators is dramatically different. In fact, irradiation of air-saturated toluene solutions of both dyes by a high power 468 nm LED resulted in no visible degradation of Pt−B2 even after 90 min of continuous irradiation (Figure 3). In the same conditions, 32% of Pd-3NF was destroyed.

Interestingly, intramolecular bridging of Pt-TTTBPtBu also results in formation of other species (Pt-B3 and Pt−B4, SI) as byproducts of Pt-B2. These phosphorescent dyes feature even longer absorption (>710 nm) and emission maxima (>950 nm) but significantly lower phosphorescence brightness (QYs ~ 1%). Although the structure of these compounds could not be elucidated so far, optimization of the synthetic procedure and variation of used precursors may possibly provide important insights in future.

Optical Oxygen Sensor. NIR phosphorescent properties of the new bridged dye enable preparation of a new generation of optical oxygen sensors. Pt-B2 was embedded into polystyrene as a model matrix (0.5 wt % indicator). The phosphorescence is efficiently quenched by oxygen (Figure 4). Nonlinear Stern−Volmer plots are typical for most oxygen sensors and can be explained by heterogeneity of the indicator environment.[33] "Two site model"[33] assumes localization of an oxygen-sensitive chromophore in two different microenvironments and adequately describes the nonlinear Stern−Volmer plots even for the luminescence decay time:

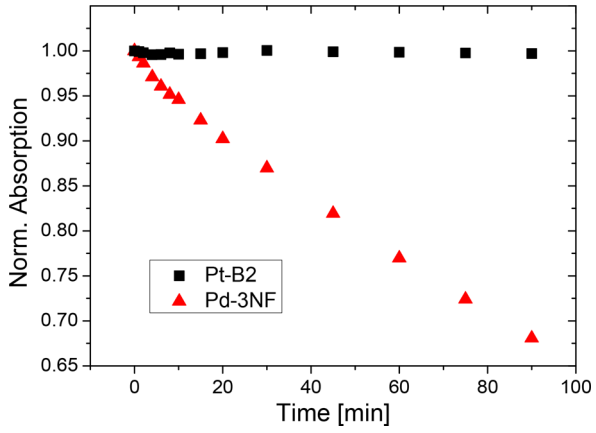

Figure 3. Photodegradation profiles for air-saturated toluene solutions of Pt-B2 and Pd-3NF (25 °C) upon irradiation with a high power blue LED array (λ_{max} = 468 nm; 10.79 V, 0.689 A, 7.4 W, photon flux: 5000 μmol s^{-1} m^{-2}).

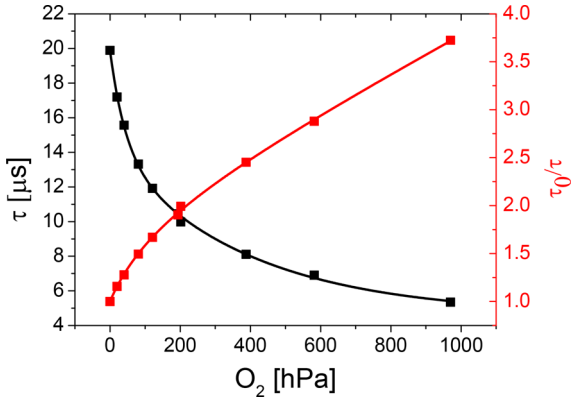

Figure 4. Lifetime and Stern−Volmer plot of Pt-B2 dissolved in polystyrene (25 °C).

$$\frac{\tau_0}{\tau} = \frac{1}{\frac{f}{1 + K_{SV1} * pO_2} + \frac{1 - f}{1 + (K_{SV1} * m) * pO_2}} \quad (1)$$

where τ_0 and τ are the lifetimes of the indicator in the absence and presence of oxygen, K_{SV1} and $K_{SV1} \cdot m$ are the Stern−Volmer constants for the first and the second site, respectively, and f is the fraction of the total emission for the first site.

DOI: 10.1021/acs.analchem.7b04760
Anal. Chem. 2018, 90, 2741−2748

The value of the Stern–Volmer constant K_{SV1} = 0.0145 hPa^{-1} is consistent with the oxygen permeability of polystyrene and the decay time of the indicator. Such sensitivity is optimal for measurement in physiologically relevant conditions. To obtain more sensitive sensors, matrixes with higher oxygen permeability (e.g., ethylcellulose, Ormosils, etc.) can be used. Favorable spectral properties make the new oxygen sensor particularly promising for in vivo oxygen monitoring due to low attenuation of the red and NIR light in tissues. Moreover, the new material may become a valuable tool for pO_2 monitoring in photosynthetic systems since its long-wavelength emission, in contrast to that of the precursor, does not overlap with that of chlorophylls and bacteriochlorophylls (Figure S15, SI).

Oxygen Flux Optode for Glucose Sensing. In contrast to the previous concepts[12,15,20] representing sensor arrays, the new glucose sensor consists of only one sensor element including three different layers (Figure 5). The general design

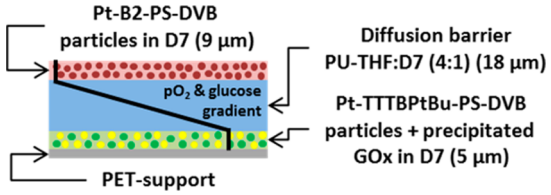

Figure 5. Cross-section of the oxygen flux optode. The thickness of the individual layers is an estimation since some intermixing occurs during the coating process.

follows the concept of the oxygen flux optode[34–37] with enzyme glucose oxidase (GOx) as an additional component. The ground layer is composed of the oxygen-sensitive microspheres (poly(styrene-*co*-divinylbenzene) doped with Pt(II) tetraphenyltetra(*t*-butyl)tetrabenzo-porphyrin, Pt-TTTBPtBu-PS-DVB) and microparticles of GOx dispersed in polyurethane hydrogel D7 and coated on a poly(ethylene terephthalate) (PET) support. Comparably large amount of GOx (9 wt %) ensures stable performance of the material despite decrease of enzyme activity with time. In the presence of glucose, oxygen is consumed:

$$\beta\text{-D-glucose} + O_2 \xrightarrow{\text{GOx}} \text{D-glucono-}\beta\text{-lactone} + H_2O_2 \quad (2)$$

The function of the second layer is to provide the diffusion barrier for glucose and oxygen in order to ensure that (i) response of the sensor is determined by mass transfer rather than by the reaction catalyzed by the enzyme, that is, all glucose molecules reaching the first layer will be converted to the products, and (ii) a gradient of oxygen is established as a result of this conversion. Overall, the layer allows to adjust the dynamic range of the sensor to physiologically relevant conditions. Unfortunately, none of the investigated commercially available materials was able to fulfill the required properties showing either too high or too low permeability for the reactants. For instance, polyurethane hydrogel D7 was found to be an adequate diffusion barrier only at 25 °C but failed at 37 °C due to higher degree of water uptake (35 and 46% water uptake, respectively) and therefore higher permeability for glucose. To address this challenge, we prepared significantly more hydrophobic polyurethane (abbreviated as PU-THF) by polycondensation of 1,4-butandiol and polytetrahydrofuran with dicyclohexylmethane-4,4′-diisocyanate. The new polymer does not show a measurable water uptake and is therefore impermeable for glucose. Whereas it is not suitable as a diffusion barrier on its own, blending with hydrogel D7 allows for adjustment of the permeability in desired range.

The top layer consists of the second type of oxygen sensitive microspheres (Pt-B2 embedded into PS-DVB) dispersed in D7 hydrogel and is necessary for compensation of the O_2 cross-talk of the glucose biosensor. The obtained signal of the sensor corresponding to the glucose levels is the difference between the oxygen levels (ΔpO_2) measured by the two oxygen sensing elements. This difference originates from the oxygen gradient (Figure 5) in the diffusion barrier established due to oxygen depletion in the enzymatic reaction in the first layer.

Optical Setup for the Read-out of the Flux Sensor. Ideally, any optical cross-talk between the two indicators used in the flux optode should be avoided, but this condition was not fully met in the previously reported systems.[15,20] Combination of the new NIR indicator with Pt-TTTBPtBu dye makes it possible to overcome this limitation. Interrogation of the optode is possible with previously reported compact phase fluorometer BiLuMOS equipped with two LEDs for excitation and two emission channels. Although the main components of the device are the same as described previously,[20] the excitation sources were adapted for the new set of indicators. In the optical setup (Figure 6), the Pt-B2-based material is excited

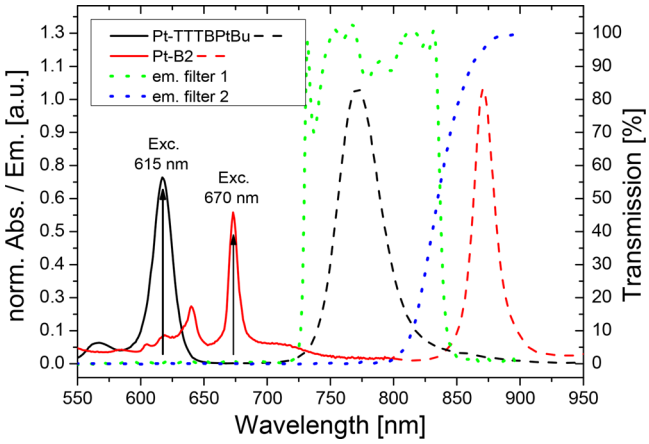

Figure 6. Spectral properties of the oxygen indicators used in the flux sensor and the optical components of the read-out device. Absorption spectra (solid lines) of Pt-TTTBPtBu and Pt-B2 and the peak excitation of the LEDs. Emission spectra (dashed lines) of the indicators and transmission spectra (dotted lines) of the respective optical filters.

with a 670 nm LED. Importantly, Pt-TTTBPtBu does not absorb at all at this wavelength. On the other hand, Pt-TTTBPtBu is efficiently excited with a 615 nm LED. Despite that Pt-B2 shows some absorption at this wavelength, the resulting minor cross-talk can be eliminated by using a band-pass filter in the Pt-TTTBPtBu detection channel (Figure 6). A simple long-pass filter (RG830; Schott, Germany) in combination with plastic filter ("Medium-Blue", Lee, U.S.A.) is sufficient to isolate the emission of Pt-B2. In order to compensate for the lower brightness of Pt-B2 and achieve comparable signals, the concentration of the Pt-B2-PS-DVB microspheres was higher than Pt-TTTBPtBu-PS-DVB microbeads.

Sensor Response. Figure 7a shows the response of the flux optode to glucose. Evidently, oxygen sensors in both layers show identical readings in the absence of glucose. As expected,

DOI: 10.1021/acs.analchem.7b04760
Anal. Chem. 2018, 90, 2741–2748

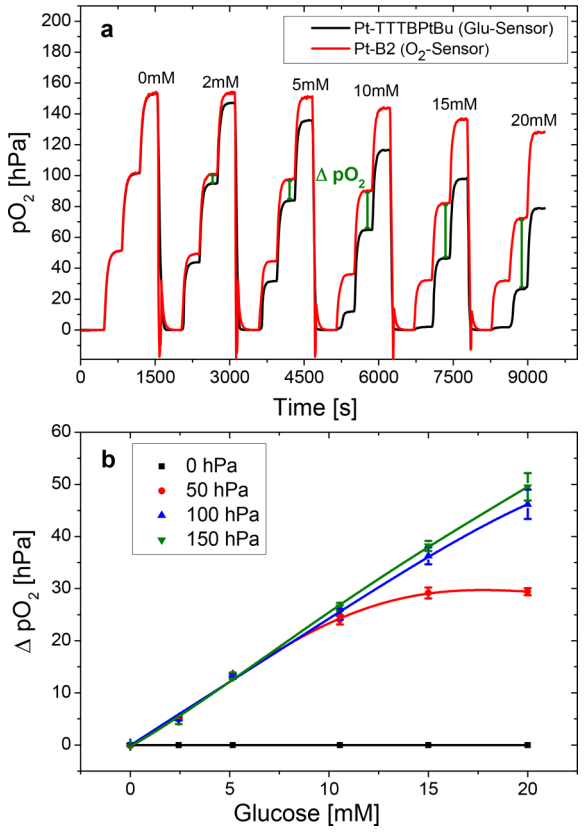

Figure 7. (a) Dynamic response of the sensor element to glucose from 0 to 20 mM in a continuous-flow measurement at different pO_2 from 0 to 150 hPa pO_2 at 37 °C. Calculated mean ΔpO_2 values for three independent measurements (three different sensor spots over a period of 3 weeks).

pO_2 measured by the particles in the first layer decreases as the glucose concentration increases. On the other hand, the pO_2 readings in the upper layer are also minor affected by glucose. Nevertheless, even in the current design the difference between the two oxygen levels (ΔpO_2) measured by both bead types shows excellent correlation to glucose levels (Figure 7b) at pO_2 values from 50 to 150 hPa. Notably, the plots of ΔpO_2 versus C(glucose) are almost linear between 100 and 150 hPa pO_2. According to Simonsen et al., the mean intercellular subcutaneous pO_2 is 74.8 ± 5.2 hPa, with potential fluctuations up to ±21 hPa,[38] which is within the range covered by the new optode. In respect to glucose concentrations, the new sensor covers the physiologically relevant range from hypoglycemia (<40 mg/dL; 2.4 mM) to hyperglycemia (>140 mg/dL; 7.8 mM).

The new sensor operates fully reversibly with ΔpO_2 returning to original values as the glucose is removed. Homogeneity of the multilayered sensor as well as the stability of the components proved to be sufficient for practical applications. In fact, the mean values in the calibration plots presented in Figure 7b were acquired for three different sensor spots originating from the same foil over a period of 3 weeks (foil was stored in a fridge at 5 °C in darkness). Moreover, the long-term stability of the glucose sensor in solution at 37 °C was investigated over a period of 18 days (Figures S29 and S30, SI). The sensor remains fully operable during this period, which indicates that no significant degradation in enzyme activity or leaching of the enzyme occurs. Interestingly, the calibration curve slightly changes in the first 5 days, which is likely to be due to rearrangement of the components in the diffusion barrier affecting its permeability for glucose and oxygen. After this initial period of time, the sensor performance is remarkably stable over the next 2 weeks, suggesting that measurement for even longer periods will also be possible. Although the enzymatic activity is known to be pH-dependent, the response of the sensor is not affected by pH (Figure S26, SI). Evidently, the sensor can tolerate some change in enzyme activity caused by pH changes, enzyme degradation and other factors due to the fact that the enzyme is present in a large excess compared to the amount needed for conversion of the glucose molecules reaching the enzymatic layer.

Temperature affects the response of all chemo- and biosensors, and the new flux optode is no exception. The origin of the temperature crosstalk is rather complex, affecting not only the diffusion rate of glucose and oxygen, but also the rate of the enzyme-catalyzed reaction as well as the sensitivity of the oxygen transducer.[20] Both oxygen sensing components show typical minor response to temperature which affects the τ_0 (decreases with temperature) and the K_{SV} (more efficient quenching at higher temperatures, Table S2 and Figure S23, SI). These effects are known and can be compensated for. As mentioned above, effect of temperature on the enzymatic activity is likely not to affect the sensor response. We observed a slight increase of ΔpO_2 values at 32 °C compared to 37 and 42 °C (Figure S28, SI) attributed to lower oxygen permeability of the diffusion barrier at lower temperatures. In fact, when the glucose sensor (no upper oxygen-sensing layer) was exposed to the rapid changes in the pO_2 (0−200 hPa, no added glucose) the dynamic response times t_{90} decreased with temperature (15.2, 11.9, and 10.7 s for 32, 37, and 42 °C, respectively).

Although the dynamic range of the sensor can be further adjusted by variation of the thickness of the diffusion barrier (higher dynamics in ΔpO_2 for thicker layers, Figure S24, SI), and its composition, the presented design already demonstrates suitability of the new sensing concept for oxygen-compensated glucose sensing in physiologically relevant range.

CONCLUSIONS

We presented a new concept of glucose quantification which is based on the use of a single optode composed of two optical oxygen sensing layers. In course of the enzymatic reaction, oxygen in the lowest layer located in proximity of the support and the enzyme is depleted, giving rise to the difference of the pO_2 values measured by the two sensing components. To make the concept suitable for subcutaneous sensing of glucose, a pair of NIR phosphorescent indicators is selected to achieve complete spectral separation of the luminescence signals. Whereas the first indicator is a conventional Pt(II) benzoporphyrin dye, the second dye belongs to a new group of phosphorescent emitters. A photostable bridged benzoporphyrin obtained via intramolecular Scholl reaction features absorption and NIR phosphorescence which are bathochromically shifted by about 60 and 110 nm, respectively, compared to the parent benzoporphyrin dye. By careful selection of the indicator chemistry and the composition of the diffusion barrier based on new polyurethane PU-THF, we were able to demonstrate oxygen-compensated glucose sensing under physiological conditions in the dynamic range of interest, covering potential hypo- and hyperglycemic events. Therefore, the new approach is expected to be of high potential for development of new generation of glucose optodes for diabetic

DOI: 10.1021/acs.analchem.7b04760
Anal. Chem. 2018, 90, 2741−2748

patients. It is also likely to be of interest for design of other types of enzymatic sensors based on oxygen transducers, such as oxygen-compensated lactate sensors.

■ ASSOCIATED CONTENT

Supporting Information

The Supporting Information is available free of charge on the ACS Publications website at DOI: 10.1021/acs.analchem.7b04760.

Synthesis, photophysical properties, DFT calculations, temperature dependency of dyes and sensor, stability tests, ^{1}H and ^{13}C NMR and mass spectra (PDF).

■ AUTHOR INFORMATION

Corresponding Author

*E-mail: sergey.borisov@tugraz.at.

ORCID

Oliver T. Hofmann: 0000-0002-2120-3259

Sergey M. Borisov: 0000-0001-9318-8273

Notes

The authors declare no competing financial interest.

■ ACKNOWLEDGMENTS

The support from Prof. Robert Saf and Ing. Karin Bartl (ICTM, TU Graz) in the acquisition of the MS-Spectra, Magdalena Traber, Maximilian Maierhofer, Anna Walcher, Christoph Staudinger, Lisa Schickhofer, Elise Hecht, and Ya Jie Knöbl for synthesis is gratefully acknowledged. The work was financially supported by the ERC Project "Oxygen" (Grant Number 267233) and the European Union FP7 Project "SenseOcean" (Grant Number 614141).

■ REFERENCES

(1) Steiner, M.-S.; Duerkop, A.; Wolfbeis, O. S. *Chem. Soc. Rev.* **2011**, *40* (9), 4805−4839.

(2) WHO | Diabetes; http://www.who.int/mediacentre/factsheets/fs312/en/ (accessed Nov 7, 2017).

(3) Heller, A.; Feldman, B. *Chem. Rev.* **2008**, *108* (7), 2482−2505.

(4) Cummins, B. M.; Garza, J. T.; Coté, G. L. *Anal. Chem.* **2013**, *85* (11), 5397−5404.

(5) Barone, P. W.; Strano, M. S. *In Vivo Glucose Sensing*; John Wiley & Sons, Inc., 2009; pp 317−329.

(6) Mader, H. S.; Wolfbeis, O. S. *Microchim. Acta* **2008**, *162* (1−2), 1−34.

(7) Pasic, A.; Koehler, H.; Schaupp, L.; Pieber, T. R.; Klimant, I. *Anal. Bioanal. Chem.* **2006**, *386* (5), 1293−1302.

(8) Marazuela, M.; Moreno-Bondi, M. *Anal. Bioanal. Chem.* **2002**, *372* (5−6), 664−682.

(9) Borisov, S. M.; Wolfbeis, O. S. *Chem. Rev.* **2008**, *108* (2), 423−461.

(10) Wang, X.; Wolfbeis, O. S. *Chem. Soc. Rev.* **2014**, *43* (10), 3666−3761.

(11) Li, L.; Walt, D. R. *Anal. Chem.* **1995**, *67* (20), 3746−3752.

(12) Pasic, A.; Koehler, H.; Klimant, I.; Schaupp, L. *Sens. Actuators, B* **2007**, *122* (1), 60−68.

(13) Wolfbeis, O. S.; Oehme, I.; Papkovskaya, N.; Klimant, I. *Biosens. Bioelectron.* **2000**, *15* (1−2), 69−76.

(14) Rumpler, M.; Hajnsek, M.; Baumann, P.; Pieber, T. R.; Klimant, I. *J. Clin. Monit. Comput.* **2017**, 1−4.

(15) Rumpler, M.; Mader, J. K.; Fischer, J. P.; Thar, R.; Granger, J. M.; Deliane, F.; Klimant, I.; Aberer, F.; Sinner, F.; Pieber, T. R.; Hajnsek, M. *Biosens. Bioelectron.* **2017**, *88* (Supplement C), 240−248.

(16) Weissleder, R. *Nat. Biotechnol.* **2001**, *19* (4), 316−317.

(17) Vinogradov, S. A.; Wilson, D. F. *J. Chem. Soc., Perkin Trans. 2* **1995**, No. 1, 103.

(18) Napp, J.; Behnke, T.; Fischer, L.; Würth, C.; Wottawa, M.; Katschinski, D. M.; Alves, F.; Resch-Genger, U.; Schäferling, M. *Anal. Chem.* **2011**, *83* (23), 9039−9046.

(19) Koo Lee, Y.-E.; Ulbrich, E. E.; Kim, G.; Hah, H.; Strollo, C.; Fan, W.; Gurjar, R.; Koo, S.; Kopelman, R. *Anal. Chem.* **2010**, *82* (20), 8446−8455.

(20) Nacht, B.; Larndorfer, C.; Sax, S.; Borisov, S. M.; Hajnsek, M.; Sinner, F.; List-Kratochvil, E. J. W.; Klimant, I. *Biosens. Bioelectron.* **2015**, *64*, 102−110.

(21) Borisov, S. M.; Zenkl, G.; Klimant, I. *ACS Appl. Mater. Interfaces* **2010**, *2* (2), 366−374.

(22) Finikova, O. S.; Aleshchenkov, S. E.; Briñas, R. P.; Cheprakov, A. V.; Carroll, P. J.; Vinogradov, S. A. *J. Org. Chem.* **2005**, *70* (12), 4617−4628.

(23) Niedermair, F.; Borisov, S. M.; Zenkl, G.; Hofmann, O. T.; Weber, H.; Saf, R.; Klimant, I. *Inorg. Chem.* **2010**, *49* (20), 9333−9342.

(24) Sommer, J. R.; Farley, R. T.; Graham, K. R.; Yang, Y.; Reynolds, J. R.; Xue, J.; Schanze, K. S. *ACS Appl. Mater. Interfaces* **2009**, *1* (2), 274−278.

(25) Kumar, R.; Ohulchanskyy, T. Y.; Roy, I.; Gupta, S. K.; Borek, C.; Thompson, M. E.; Prasad, P. N. *ACS Appl. Mater. Interfaces* **2009**, *1* (7), 1474−1481.

(26) Cheprakov, A. V.; Filatov, M. A. *J. Porphyrins Phthalocyanines* **2009**, *13* (03), 291−303.

(27) Hutter, L. H.; Müller, B. J.; Koren, K.; Borisov, S. M.; Klimant, I. *J. Mater. Chem. C* **2014**, *2* (36), 7589−7598.

(28) Zach, P. W.; Freunberger, S. A.; Klimant, I.; Borisov, S. M. *ACS Appl. Mater. Interfaces* **2017**, *9* (43), 38008−38023.

(29) Rempala, P.; Kroulík, J.; King, B. T. *J. Org. Chem.* **2006**, *71* (14), 5067−5081.

(30) Rempala, P.; Kroulík, J.; King, B. T. *J. Am. Chem. Soc.* **2004**, *126* (46), 15002−15003.

(31) Waldvogel, S. R.; Trosien, S. *Chem. Commun.* **2012**, *48* (73), 9109.

(32) Lu, Y.; Moore, J. S. *Tetrahedron Lett.* **2009**, *50* (28), 4071−4077.

(33) Carraway, E. R.; Demas, J. N.; DeGraff, B. A.; Bacon, J. R. *Anal. Chem.* **1991**, *63* (4), 337−342.

(34) Holst, G. A.; Köster, T.; Voges, E.; Lübbers, D. W. *Sens. Actuators, B* **1995**, *29* (1), 231−239.

(35) Lübbers, D. W. *Sens. Actuators, B* **1993**, *11* (1), 253−262.

(36) Stücker, M.; Altmeyer, P.; Struk, A.; Hoffmann, K.; Schulze, L.; Röchling, A.; Lübbers, D. W. *J. Invest. Dermatol.* **2000**, *114* (3), 533−540.

(37) Hartmann, P.; Ziegler, W.; Holst, G.; Lübbers, D. W. *Sens. Actuators, B* **1997**, *38* (1), 110−115.

(38) Simonsen, L.; Bülow, J.; Madsen, J. *Am. J. Physiol.* **1994**, *266* (3), E357−365.

DOI: 10.1021/acs.analchem.7b04760
Anal. Chem. 2018, 90, 2741−2748